

Impact of oil spills on mangrove ecosystem degradation in the Niger Delta using remote sensing and machine learning

Erebi Lisa Jonathan^{1,*}, Okes Imoni², Prince Chukwuemeka², Desmond Rowland Eteh¹

¹ Department of Geology, Niger Delta University, Amassoma 560103, Nigeria

² Department of Biological Sciences, Niger Delta University, Amassoma 560103, Nigeria

* **Corresponding author:** Jonathan Lisa Erebi, jonathanlisa788@gmail.com

CITATION

Jonathan EL, Imoni O, Chukwuemeka P, Eteh DR. Impact of oil spills on mangrove ecosystem degradation in the Niger Delta using remote sensing and machine learning. *Journal of Geography and Cartography*. 2025; 8(2): 11707.
<https://doi.org/10.24294/jgc11707>

ARTICLE INFO

Received: 23 April 2025

Accepted: 3 June 2025

Available online: 17 June 2025

COPYRIGHT



Copyright © 2025 by author(s).

Journal of Geography and Cartography is published by EnPress Publisher, LLC. This work is licensed under the Creative Commons Attribution (CC BY) license.
<https://creativecommons.org/licenses/by/4.0/>

Abstract: Mangrove forests are vital to coastal protection, biodiversity support, and climate regulation. In the Niger Delta, these ecosystems are increasingly threatened by oil spill incidents linked to intensive petroleum activities. This study investigates the extent of mangrove degradation between 1986 and 2022 in the lower Niger Delta, specifically the region between the San Bartolomeo and Imo Rivers, using remote sensing and machine learning. Landsat 5 TM (1986) and Landsat 8 OLI (2022) imagery were classified using the Support Vector Machine (SVM) algorithm. Classification accuracy was high, with overall accuracies of 98% (1986) and 99% (2022) and Kappa coefficients of 0.97 and 0.98. Healthy mangrove cover declined from 2804.37 km² (58%) to 2509.18 km² (52%), while degraded mangroves increased from 72.03 km² (1%) to 327.35 km² (7%), reflecting a 354.46% rise. Water bodies expanded by 101.17 km² (5.61%), potentially due to dredging, erosion, and sea-level rise. Built-up areas declined from 131.85 km² to 61.14 km², possibly reflecting socio-environmental displacement. Statistical analyses, including Chi-square ($\chi^2 = 1091.33$, $p < 0.001$) and Kendall's Tau ($\tau = 1$, $p < 0.001$), showed strong correlations between oil spills and mangrove degradation. From 2012 to 2022, over 21,914 barrels of oil were spilled, with only 38% recovered. Although paired *t*-tests and ANOVA results indicated no statistically significant changes at broad scales, localized ecological shifts remain severe. These findings highlight the urgent need for integrated environmental policies and restoration efforts to mitigate mangrove loss and enhance sustainability in the Niger Delta.

Keywords: conservation; land cover change; machine learning; mangrove degradation; Niger Delta; oil spills; remote sensing; Support Vector Machine (SVM)

1. Introduction

Mangrove forest ecosystems are among the most ecologically and economically significant coastal environments, providing a range of critical ecosystem services. These include coastal protection, carbon sequestration, biodiversity conservation, fisheries support, and contributions to local livelihoods through timber, fuelwood, and other forest products [1–3]. As blue carbon ecosystems, mangroves play a pivotal role in mitigating climate change by acting as effective carbon sinks, storing substantial amounts of carbon in their biomass and sediments. They also serve as natural buffers against coastal erosion, storm surges, and rising sea levels, which are becoming increasingly prevalent due to anthropogenic climate change. Despite their immense ecological value, mangrove forests are among the most threatened ecosystems globally, facing severe degradation due to a combination of anthropogenic activities, including oil exploration, pollution, deforestation, land reclamation, and the expansion of aquaculture [4,5]. These threats have led to significant losses in mangrove cover,

diminishing their ecological integrity and functionality [6,7]. Understanding the spatiotemporal patterns of mangrove degradation, particularly in response to oil spills, is essential for effective conservation, restoration, and management of these fragile ecosystems. The Niger Delta, one of the largest wetland and mangrove ecosystems in Africa, covers approximately 76,000 km², with its mangroves extending across an estimated 11,000 km² [1]. It supports an extensive range of biodiversity and provides critical socio-economic benefits to local communities. However, it is also one of the most heavily degraded mangrove ecosystems in the world due to industrial activities, particularly those associated with the oil and gas sector [4,5,8]. Since the discovery of oil in the late 1950s, the Niger Delta has experienced frequent oil spills, which have had devastating consequences for the region's mangrove forests. In addition to direct contamination, other oil industry activities such as dredging, pipeline construction, and the disposal of drilling waste have further exacerbated environmental degradation [8]. Illegal crude oil bunkering and the proliferation of artisanal refineries have significantly increased oil spill incidents in recent years, leading to the contamination of mangrove forests and water bodies at an alarming rate [9,10]. Despite these concerns, there remains a lack of comprehensive quantitative assessments of the extent of mangrove degradation attributable to oil spills, necessitating an in-depth spatial and temporal analysis.

Remote sensing and machine learning techniques provide powerful tools for assessing and monitoring changes in mangrove cover over time. Land cover change detection using satellite imagery has been widely applied to study ecosystem dynamics, particularly in environments vulnerable to anthropogenic disturbances [11,12]. Among various classification algorithms, Support Vector Machines (SVMs) have emerged as one of the most effective techniques for land cover classification due to their ability to handle complex, nonlinear relationships and their robustness against noise and outliers [13,14]. SVMs are particularly advantageous for analyzing mangrove ecosystems because of their ability to accurately distinguish mangroves from other land cover types using multispectral and hyperspectral data [15]. Compared to traditional classification methods such as Maximum Likelihood Classification (MLC) and Decision Trees (DTs), SVMs have consistently demonstrated superior accuracy in land cover mapping, making them a preferred choice for monitoring mangrove degradation [14,16]. The non-parametric nature of SVMs enables them to effectively model intricate spectral variations in mangrove forests, which is critical given the spectral similarities between mangroves, other coastal vegetation, and oil-affected areas [17]. Furthermore, SVMs are well-suited for handling high-dimensional satellite data, making them an optimal choice for long-term mangrove monitoring [18]. Their resilience to data noise caused by atmospheric interference during satellite acquisition ensures reliable classification results, which is crucial when analyzing multi-temporal datasets [19]. SVMs also provide clear classification outputs by delineating support vectors, allowing for precise identification of areas experiencing mangrove degradation [20]. Their ability to generalize well, even when trained on limited datasets, makes them highly effective for detecting land cover changes in new and previously unmonitored areas [21]. This study utilizes Landsat satellite imagery spanning a 36-year period (1986–2022) to analyze changes in mangrove cover in the Niger Delta, employing a Support Vector Machine (SVM) classifier for accurate

classification and change detection. The primary objectives of this research include analyzing land cover changes over the study period using Landsat imagery and an SVM classifier, evaluating the extent of mangrove degradation, and quantifying changes in both healthy and degraded mangrove cover. Additionally, the study investigates the statistical relationship between oil spill occurrences and mangrove degradation through Chi-square tests and Kendall's Tau analysis. Beyond mangroves, the research also assesses other environmental changes, such as variations in water bodies and built-up areas, and explores their potential links to anthropogenic activities. Ultimately, the study aims to provide valuable insights into conservation strategies and recommend policy interventions to mitigate mangrove loss and promote sustainable ecosystem management in the Niger Delta. The study's methodology will involve processing multi-temporal Landsat satellite imagery to classify land cover using an SVM classifier, with a particular focus on distinguishing healthy mangroves from degraded mangroves and other land cover types. Change detection analysis will be conducted to quantify the extent of mangrove loss over the study period, while statistical techniques will be employed to examine the correlation between oil spill events and observed mangrove degradation. By leveraging machine learning and geospatial analysis, this research will offer a comprehensive assessment of mangrove ecosystem health in the Niger Delta, shedding light on the specific impacts of oil spills and other anthropogenic pressures. The findings will provide critical insights for policymakers, conservationists, and stakeholders engaged in ecosystem restoration and sustainable environmental management. Ultimately, this study aims to contribute to a deeper understanding of how oil spills influence mangrove ecosystem degradation in the Niger Delta and inform evidence-based conservation and policy interventions. By integrating advanced remote sensing and machine learning techniques with robust statistical analysis, the research seeks to bridge knowledge gaps in mangrove ecosystem monitoring and support the implementation of effective conservation strategies. Given the growing environmental and socio-economic implications of mangrove loss, the results of this study will be instrumental in advocating for stronger environmental policies and remediation measures to safeguard the Niger Delta's mangrove ecosystems for future generations.

2. Study area

The study area is situated within the mangrove-dominated coastal wetlands of the Niger Delta, specifically along the lower reaches of the San Bartolomeo and Imo Rivers as they discharge into the Atlantic Ocean (**Figure 1**) in 4.5° N– 5.5° N and 6.5° E– 7.5° E). This region represents one of the most ecologically significant yet environmentally stressed landscapes in West Africa, characterized by extensive tidal channels, estuarine creeks, and intertidal mudflats that support highly productive mangrove ecosystems [1,22]. The region experiences substantial annual rainfall, averaging approximately 4000 mm, which plays a crucial role in groundwater recharge within the Niger Delta, and the mangrove forests, among the largest in Africa, play a crucial role in coastal protection, carbon sequestration, and biodiversity conservation [23]. However, the area is also a hub for intensive hydrocarbon exploration and production, hosting a dense infrastructure of oil wells, flow stations, pipelines, and

related facilities [24]. Decades of petroleum exploitation have led to significant ecological disturbances, including deforestation, hydrological alterations, and frequent oil spills, which threaten both the natural ecosystem and the livelihoods of indigenous communities dependent on fisheries, aquaculture, and forest resources [25]. Given the critical ecological services provided by these mangrove forests and the growing anthropogenic pressures, continuous monitoring of land cover changes is imperative for sustainable management and conservation efforts [26].

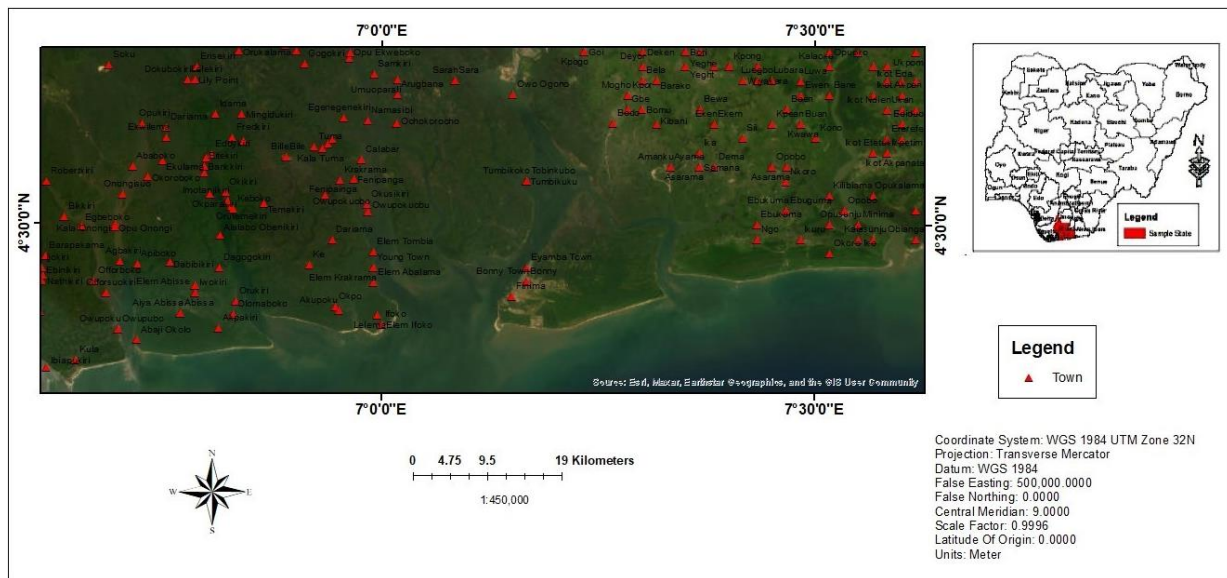


Figure 1. Study area showing towns.

3. Materials and methods

This study employed a comprehensive approach combining remote sensing, geospatial analysis, and machine learning techniques to assess mangrove cover changes in the lower Niger Delta region, specifically focusing on the San Bartolomeo River and Imo River areas using the ArcGIS version 10.5 environment and a Python program. The methodology included several key steps (**Figure 2**): data acquisition, image preprocessing, training data preparation, Support Vector Machine (SVM) classification, change detection, map generation, accuracy assessment, and statistical analysis.

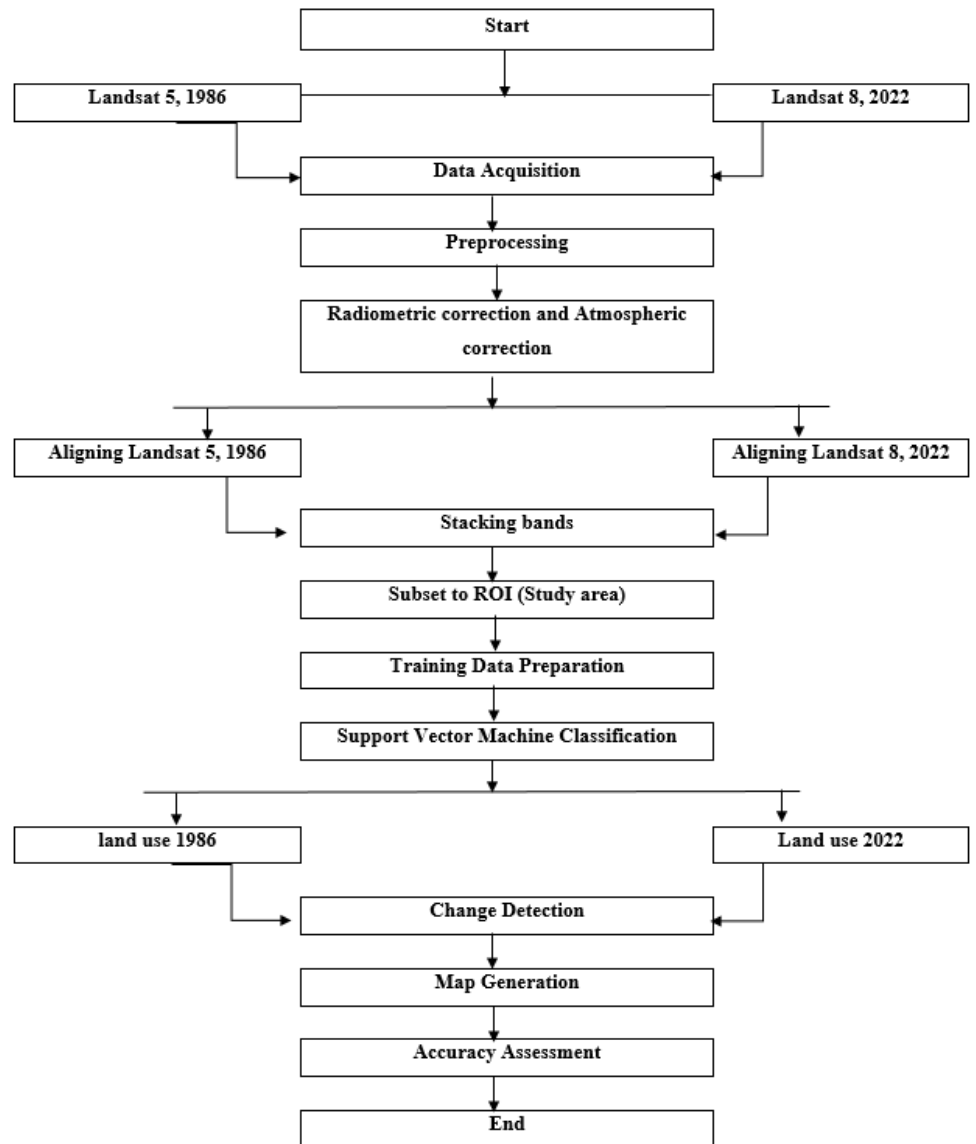


Figure 2. Data processing steps.

3.1. Data acquisition

The initial step of the study involved the acquisition of multi-temporal satellite imagery essential for land cover change detection. Landsat 5 Thematic Mapper (TM) for the year 1986 and Landsat 8 Operational Land Imager (OLI) for 2022 were obtained from the United States Geological Survey (USGS) Earth Explorer platform [27]. These datasets were selected based on their long-term availability, consistent 30-m spatial resolution, and reliability in land use/land cover (LULC) assessments across time [28,29]. Metadata files, including radiometric calibration parameters and solar geometry data, were downloaded alongside each scene to facilitate accurate preprocessing.

- Landsat 5 TM (1986): Bands 1–7, spatial resolution of 30 m.
- Landsat 8 OLI (2022): Bands 1–9, spatial resolution of 30 m.

Accompanying metadata files were obtained to ensure proper image calibration and preprocessing.

The field data using GIS and a geotagged camera for mapping of mangrove spots and non-mangrove areas to enable us to train the sample properly.

3.1.1. Field survey and ground truth data

To improve classification accuracy, fieldwork was conducted using GPS-enabled devices and a geotagged camera to map mangrove and non-mangrove zones. These geo-referenced points served as ground truth data for supervised classification. A total of 200 samples were collected, covering key LULC classes such as mangroves, degraded mangroves, built-up areas, bare land, and water bodies [30].

3.1.2. Image preprocessing

Image preprocessing is a critical step to enhance the quality and accuracy of satellite data before any analytical procedures. The following preprocessing steps were undertaken:

- 1) **Radiometric correction:** Radiometric corrections were applied to the imagery to correct sensor-related issues and atmospheric distortions. This involved converting the digital numbers (DNs) of the satellite images into top-of-atmosphere (TOA) reflectance values. The conversion process utilized the radiometric calibration coefficients available in the metadata, accounting for any sensor degradation over time. This step ensured that the reflectance values were consistent across different images, facilitating accurate comparison [31,32].

$$\text{TOA Reflectance} = \frac{\pi * L\lambda * d^2}{\text{ESUN}\lambda * \cos(\Theta_s)} \quad (1)$$

where:

- $L\lambda$ is the spectral radiance;
- d is the Earth-Sun distance in astronomical units;
- $\text{ESUN}\lambda$ is the mean solar exoatmospheric irradiance;
- Θ_s is the solar zenith angle.

Radiometric correction ensured comparability of reflectance values across temporal scenes, compensating for changes in illumination geometry and sensor characteristics.

Atmospheric correction

Atmospheric interference from water vapor, dust, and aerosols was mitigated using the Dark Object Subtraction (DOS) method, an image-based correction technique that assumes certain dark pixels (e.g., deep water) should have near-zero reflectance. This process eliminated additive atmospheric noise and improved the retrieval of surface reflectance [33,34].

Geometric correction and georeferencing

All images were geometrically corrected to ensure pixel-level alignment. Ground Control Points (GCPs) collected from high-resolution Google Earth imagery and field GPS data were used to register the images. The final georeferencing was implemented in the Universal Transverse Mercator (UTM) projection, Zone 32N, using the WGS84 datum. This process eliminated spatial distortions and ensured consistency across image dates [35].

Image stacking and subsetting

Post-correction, multispectral bands relevant to vegetation and land use classification—Red, Green, Blue, and Near-Infrared (NIR)—were extracted and stacked using ENVI. The resulting composite images were subset to a defined Region of Interest (ROI) encompassing areas of ecological and socio-economic relevance. The ROI was delineated using administrative boundaries, field coordinates, and ecological risk zones [36].

Training data preparation

Accurate classification requires high-quality training data:

Ground-truth data collection

A total of 200 georeferenced training samples were collected during fieldwork. These were categorized into mangrove, degraded mangrove, built-up, bare land, and water classes, verified visually and with historical land cover information.

Spectral signature extraction

Using ArcGIS 10.8, the spectral reflectance values for each sample point were extracted across all selected bands. The extracted values were plotted to analyze variability among classes.

Feature selection and dimensionality reduction

Principal Component Analysis (PCA) was conducted using Python (scikit-learn module) to reduce dimensionality and identify features with the highest discriminative power, following the procedure by Veraverbeke et al. [37].

Support Vector Machine (SVM) classification

The classification of land cover was performed using the Support Vector Machine (SVM) algorithm, a powerful machine-learning technique known for its effectiveness in handling high-dimensional data and small sample sizes. The classification process involved the following steps:

- 1) **Model training:** The SVM classifier was trained using the selected training dataset. The radial basis function (RBF) kernel was chosen for the SVM model due to its ability to handle non-linear relationships between features. The kernel type, along with the regularization parameter (C), was optimized through grid search and cross-validation techniques to achieve the highest possible classification accuracy.
- 2) **Classification execution:** Once trained, the SVM model was applied to the entire multiband imagery from both 1986 and 2022. The model classified each pixel into one of the predefined land cover classes, such as mangroves and non-mangroves. The classification results were then subjected to a post-processing step to remove any spurious classifications, ensuring smooth and contiguous land cover maps.

$$K(x_i, x_j) = \exp(-\gamma \|x_i - x_j\|^2) \quad (2)$$

where:

x_i and x_j are feature vectors; γ is a kernel parameter that defines the influence of a single training example.

Change detection

Change detection is a crucial step in understanding the dynamics of land cover over time. In this study, change detection focused on identifying shifts in mangrove forest cover between 1986 and 2022. The process involved:

- 1) **Comparative analysis:** The classified images from 1986 and 2022 were compared pixel by pixel to detect changes in land cover. Areas where mangroves were converted to other land cover types or vice versa were identified.
- 2) **Quantification of changes:** The extent of mangrove loss and gain was quantified by calculating the area covered by mangroves in each year. This quantification provided insights into the rate of change and the factors contributing to mangrove degradation or restoration in the study area.

Map generation

To effectively communicate the results of the study, detailed maps and visualizations were generated using ArcGIS 10.5. The map generation process included:

- 1) **Creation of land cover maps:** Land cover maps for both 1986 and 2022 were produced, highlighting the distribution of different land cover types within the study area. Special attention was given to the visualization of mangrove cover, using distinct color schemes to differentiate between areas of gain, loss, and stability.
- 2) **Change detection maps:** Change detection maps were created to visualize the spatial distribution of changes in mangrove cover. These maps provided a clear representation of areas where significant changes had occurred, enabling easy interpretation and identification of hotspots of mangrove loss or gain.
- 3) **Layout design and annotation:** The maps were designed with a clear layout, including legends, north arrows, and scale bars, to enhance readability. Annotations were added to highlight key areas and provide context to the visualizations, making the results accessible to a broad audience, including policymakers and conservationists.

Accuracy assessment

The accuracy of the land cover classification was rigorously assessed to ensure the reliability of the results. The accuracy assessment process involved:

- 1) **Validation data:** A separate set of validation data, comprising ground truth points that were not used in the training phase, was used to assess classification accuracy. These points were randomly distributed across the study area and represented all land cover classes.
- 2) **Confusion matrix:** A confusion matrix was generated by comparing the classified land cover types with the actual land cover at each validation point. This matrix provided detailed insights into the classification performance, indicating the number of correctly and incorrectly classified pixels for each class.
- 3) **Accuracy metrics:** Several accuracy metrics were calculated from the confusion matrix, including overall accuracy, producer's accuracy, and user's accuracy for each land cover class. The Kappa coefficient, which measures the agreement between the classified and actual land cover types beyond chance, was also computed. A Kappa coefficient close to unity indicated a high level of accuracy in the classification process.

- 4) Error analysis: An error analysis was conducted to identify and understand the sources of misclassification. This analysis helped refine the classification process and provided insights into potential improvements for future studies.

$$\kappa = \frac{po - pe}{1 - pe} \quad (3)$$

where:

- po is the observed accuracy,
- pe is the expected accuracy.

The Kappa coefficient close to 1 indicates a high degree of classification accuracy
Percentage change calculation

This formula is used to calculate the percentage change in land cover classes over time. It provides insight into how much an area has increased or decreased relative to its original extent in 1986. A positive value indicates an increase in land cover, while a negative value represents a loss. This approach is widely used in remote sensing and land use change studies to quantify environmental transformations. By analyzing percentage change, researchers can track forest loss, urban expansion, and hydrological changes, making it a crucial metric in landscape dynamics analysis [39].

$$\text{Percentage Change} = \left(\frac{\text{Area in 2022} - \text{Area in 1986}}{\text{Area in 1986}} \right) \times 100 \quad (4)$$

Cohen's d effect size

Cohen's d measures the magnitude of change between two datasets [40]. It standardizes the difference between the mean land cover areas in 1986 and 2022, allowing for interpretation of effect size.

$$d = \frac{\bar{X}_1 - \bar{X}_2}{s_p} \quad (5)$$

$$s_p = \sqrt{\frac{s_1^2 + s_2^2}{2}} \quad (6)$$

where:

- \bar{X}_1, \bar{X}_2 are the means of land cover areas in 1986 and 2022.
- s_1, s_2 are the standard deviations of land cover areas in 1986 and 2022.

Paired t-test statistic

The paired *t*-test determines if the difference between land cover areas in 1986 and 2022 is statistically significant. It compares two dependent datasets, assessing whether changes over time occur due to random fluctuations or actual transformation [41].

where:

- sd is the standard deviation of the differences.
- n is the number of observations.

$$t = \frac{\bar{X}_1 - \bar{X}_2}{\frac{s_d}{\sqrt{n}}} \quad (7)$$

One-way ANOVA

One-way ANOVA tests if there is a statistically significant difference between land cover areas across different years (1986 and 2022). It compares within-group variance (changes within each land cover type) against between-group variance (differences across years) [42].

Formula

$$F = \frac{\text{Between-group variance}}{\text{Within-group variance}} = \frac{\frac{\sum n_i(\bar{X}_i - \bar{X})^2}{k-1}}{\frac{\sum (x_{ij} - \bar{X}_i)^2}{N-k}} \quad (8)$$

where:

- n_i is the number of samples in each group.
- \bar{X}_i is the mean of each group.
- \bar{X} is the overall mean.
- k is the number of groups.
- N is the total number of observations.

Linear regression model

Linear regression is a fundamental statistical and machine learning technique used for modeling the relationship between a dependent variable and one or more independent variables [43]

$$Y = \beta_0 + \beta_1 X + \epsilon \quad (9)$$

where:

- Y is the land cover area.
- X is the year.
- β_0 is the intercept.
- β_1 is the slope coefficient.
- ϵ is the error term.

Oil spill data processing

Given the prevalence of oil exploration activities in the study area, data on oil spills from 2012 to 2022 were obtained from the National Oil Spill Detection and Response Agency (NOSDRA) website, <https://oilspillmonitor.ng/>. This data was processed in ArcGIS to identify spill locations, extents, and frequencies. The processed oil spill data was then correlated with the observed changes in mangrove cover to assess the impact of oil spills on the mangrove ecosystem. Statistical analyses were conducted using Python programming to visualize trends and establish relationships between oil spill incidents and mangrove degradation.

Chi-square test (χ^2)

The Chi-square test is used to determine whether there is a significant association between two categorical variables [44].

$$\chi^2 = \sum \frac{(O_i - E_i)^2}{E_i} \quad (10)$$

where:

- O_i = Observed frequency;
- E_i = Expected frequency.

Kruskal-Wallis test (H)

The Kruskal-Wallis test is a non-parametric test used to compare medians across multiple groups when normality assumptions are violated. It ranks the data instead of using raw values and calculates [45].

$$H = \frac{12}{n(n+1)} \sum \frac{R_i^2}{n_i} - 3(n+1) \quad (11)$$

where:

- n = Total number of observations
- R_i = Sum of ranks for group I
- n_i = Number of observations in group I.

Kendall's Tau (τ) trend test

The Kendall's Tau test measures the strength and direction of the trend between two variables over time [46].

$$\tau = \frac{C - D}{\frac{1}{2}n(n-1)} \quad (12)$$

where:

- C = Number of concordant pairs;
- D = Number of discordant pairs;
- n = Number of observations.

4. Results and discussion

4.1. Mangrove cover

Mangrove forests, vital for coastal protection, carbon sequestration, and biodiversity, have experienced a noticeable decline in the study area over the 36-year period. In 1986, mangrove and cover accounted for approximately 2804.37 km², or 58% of the total study area (**Table 1, Figures 3–6**). However, by 2022, this had reduced to 2509.18 km², representing 52% coverage (**Table 1, Figures 5 and 7**). This decline translates to a loss of 295.19 km², equivalent to a 6% reduction in mangrove habitat (**Table 1 and Figure 8**). In contrast, degraded mangrove areas increased significantly, from 72.03 km² (1%) in 1986 to 327.35 km² (7%) in 2022, a gain of 255.32 km², or 6% (**Table 1 and Figure 8**). The decline in healthy mangroves and the corresponding rise in degraded mangroves raises serious concerns. Mangrove degradation can adversely affect biodiversity, reducing habitat availability for numerous species and undermining the ecosystem services provided by mangroves, such as coastal erosion control and carbon storage. This trend underscores the urgent need for a detailed investigation into the drivers of mangrove loss. Anthropogenic activities, including deforestation, oil exploration, and urban expansion, are likely contributors. Changes in hydrological patterns due to climate change or human interventions, such as canal dredging for the petroleum industry, exacerbate the issue.

Table 1. Results from Support Vector Machine classification in the study area.

Classification	1986 km ²	1986 %	2022 km ²	2022 %	Gain/Loss km ²	Percentage Change
Mangrove	2804.37	58	2509.18	52	-295.19	-10.5261
Degraded Mangrove	72.03	1	327.35	7	255.32	354.4634
Bare land	35.49	1	46.9	1	11.41	32.1499
Built up area	131.85	3	61.14	1	-70.71	-53.6291
Waterbody	1803.45	37	1904.62	39	101.17	5.609803

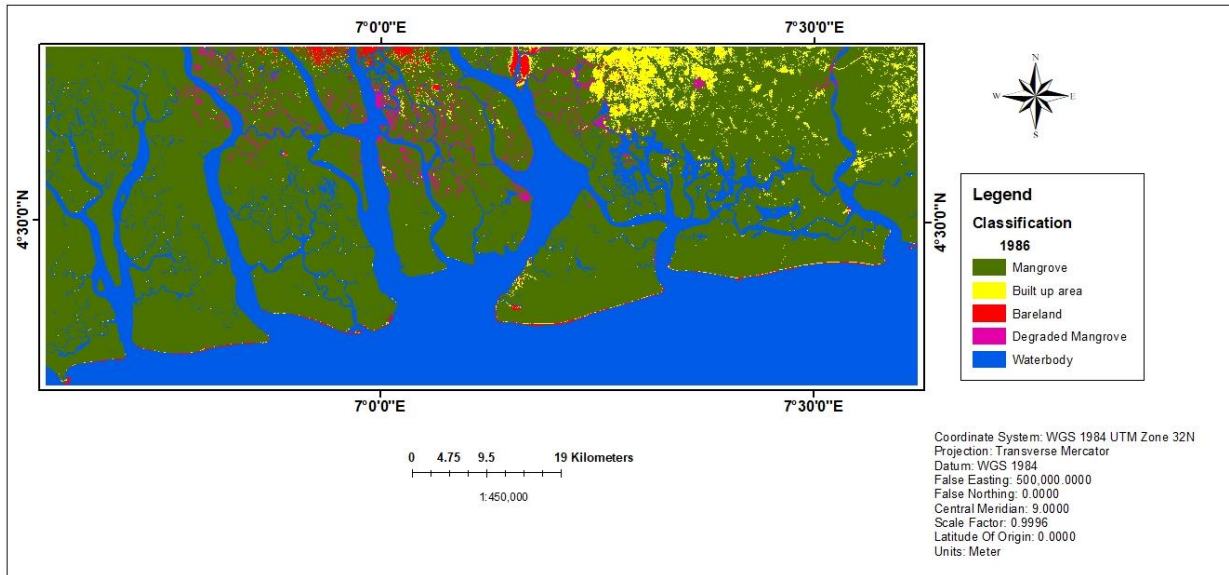


Figure 3. Land cover in the study area 1986.

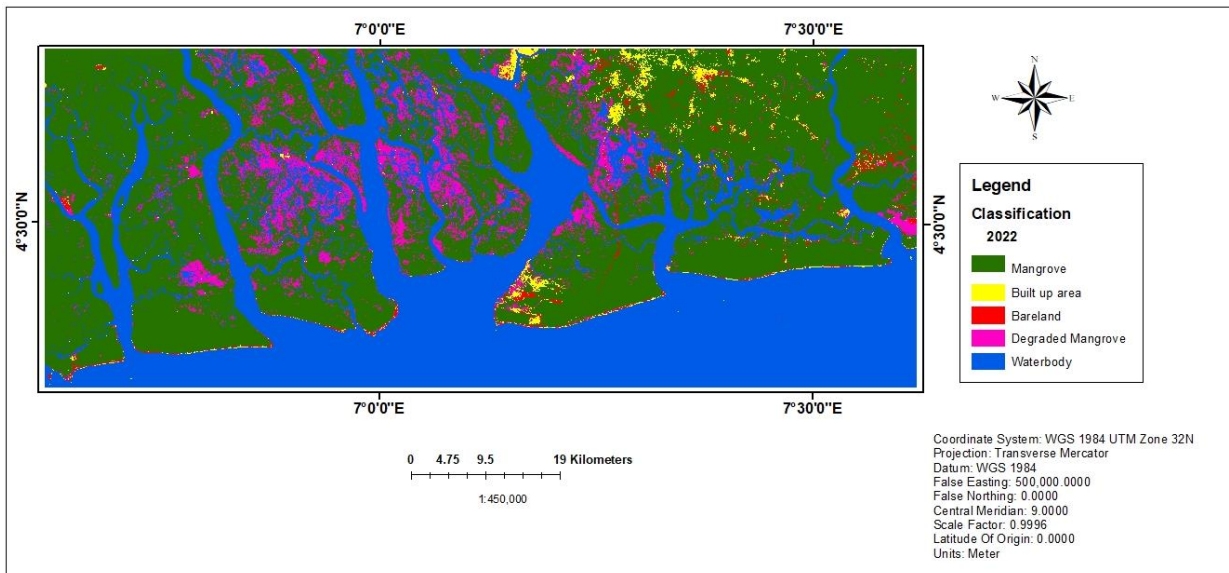


Figure 4. Land cover in the study area 2022.

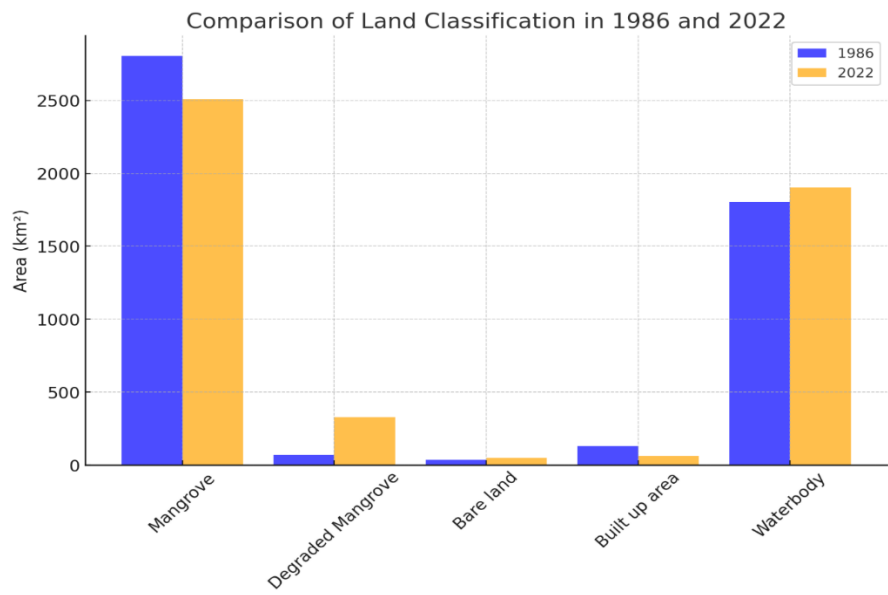


Figure 5. Comparison of land classification in 1986 and 2022.

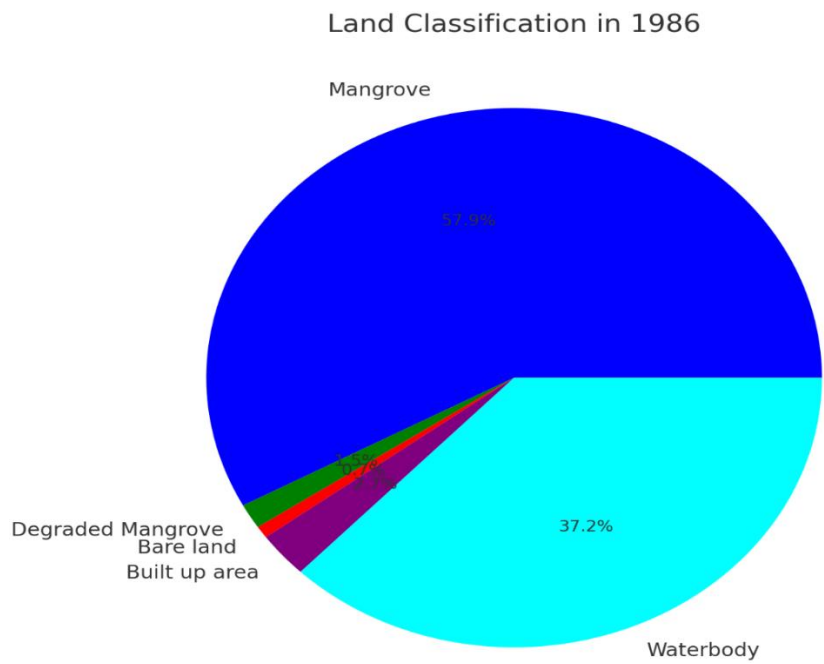


Figure 6. Land classification in 1986.

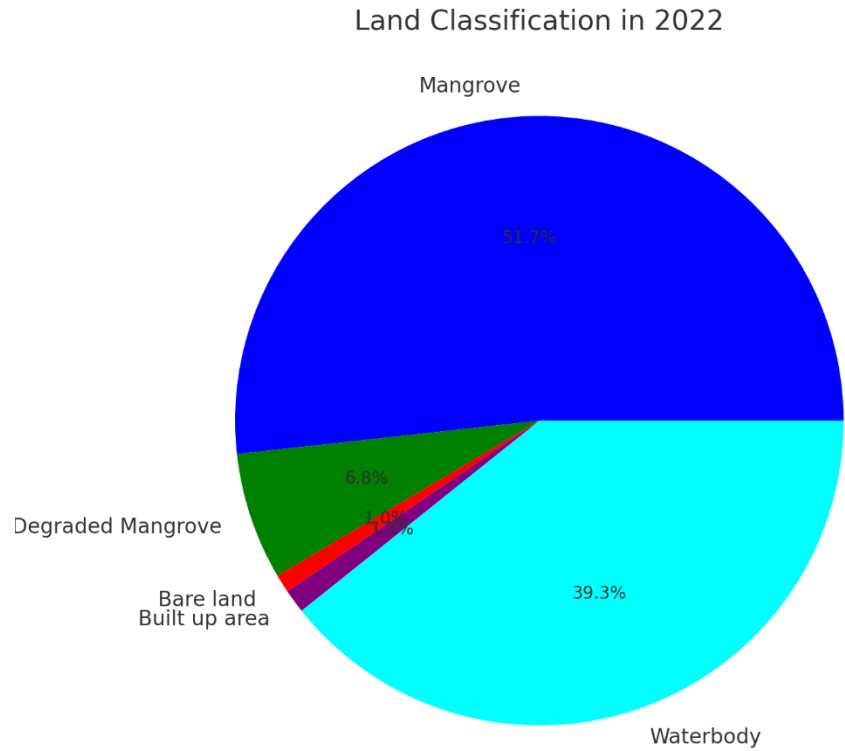


Figure 7. Land classification in 2022.

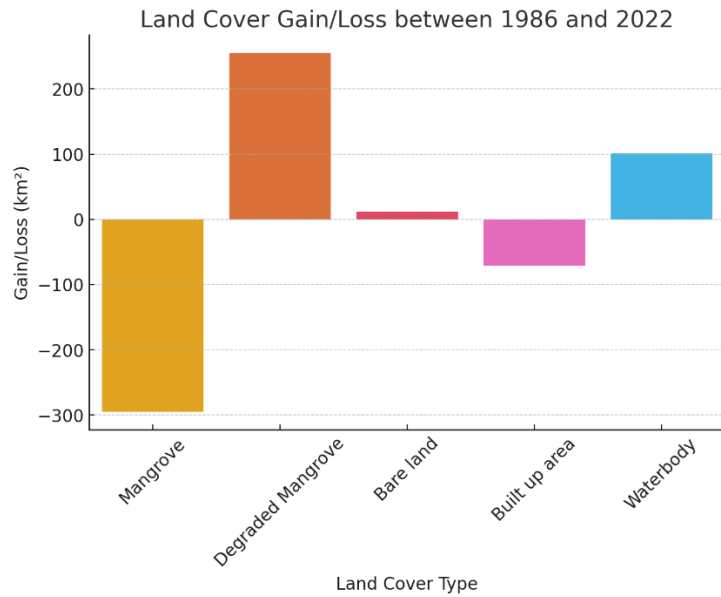


Figure 8. Land cover gain /loss between 1986 and 2022.

4.2. Waterbody dynamics

During the same study period, waterbody cover increased from 1803.45 km² (37%) in 1986 to 1904.62 km² (39%) in 2022, reflecting a gain of 101.17 km², which is about a 2% increase in **Table 1**, **Figures 5** and **8**. Changes in waterbody dynamics can have cascading effects on the entire ecosystem, affecting hydrological cycles, aquatic habitats, and overall ecosystem resilience [47]. The rise in waterbody cover emphasizes the need for comprehensive studies on the drivers of this change. Factors such as climate patterns, land-use practices, and human interventions in water

management should be explored to understand the implications for biodiversity and ecosystem health. However, the petroleum industry is known to carry out both capital and routine maintenance dredging in support of their exploration activities. Oil industry access canals have been shown to increase water bodies while decreasing mangrove cover and have been shown to cause hydrological and microtopographic changes [47]. Ohimain et al. [48] demonstrated how abandoned dredged spoils support the replacement of former mangrove cover with non-mangroves.

4.3. Built-up areas

Contrary to the global trend of urban expansion, built-up areas in the study region decreased significantly over the study period. In 1986, built-up areas occupied 131.85 km², or 3% of the total area (**Table 1** and **Figure 6**). By 2022, this had declined to 61.14 km², representing only 1% of the area in **Table 1** and **Figure 7**. This 70.71 km² reduction in built-up areas, or a 2% decrease, is an intriguing finding that raises questions about urbanization dynamics and land-use policies in the region in **Figure 8**. The decline in built-up areas may be influenced by several factors, including environmental regulations, economic shifts, or the relocation of settlements due to environmental degradation or flooding. The Niger Delta is prone to severe flooding, which could have prompted the abandonment or relocation of certain settlements. Additionally, sociopolitical factors, such as land tenure issues or community displacement, may have played a role.

4.4. Bare land cover

Bare land, a relatively minor land cover class in the region, showed a modest increase over the study period. In 1986, bare land accounted for 35.49 km², or 1% of the total area (**Table 1** and **Figure 6**). By 2022, this had increased slightly to 46.9 km², still representing 1% of the area (**Table 1** and **Figure 7**). This gain of 11.41 km² may seem minor compared to the changes in other land cover classes (**Figure 8**), but it warrants attention due to its potential implications for ecosystem stability. Changes in bare land can affect soil erosion, habitat loss, and overall landscape stability. The modest increase observed in this study may be linked to specific land management practices or natural ecological processes. For example, areas cleared for agriculture or construction that were later abandoned could contribute to the rise in bare land. Monitoring these changes is essential for understanding their broader ecological and environmental implications.

4.5. Percentage change analysis

The percentage change in land cover classes over the 36-year period highlights significant ecological shifts in **Table 1** and **Figure 9**. The mangrove forest witnessed a 10.53% decline, losing 295.19 km² (**Table 1** and **Figure 10**). This is concerning, as mangroves serve as essential coastal barriers and carbon sinks. The factors contributing to this decline could be deforestation for fuelwood, aquaculture, coastal development, and natural climatic changes.

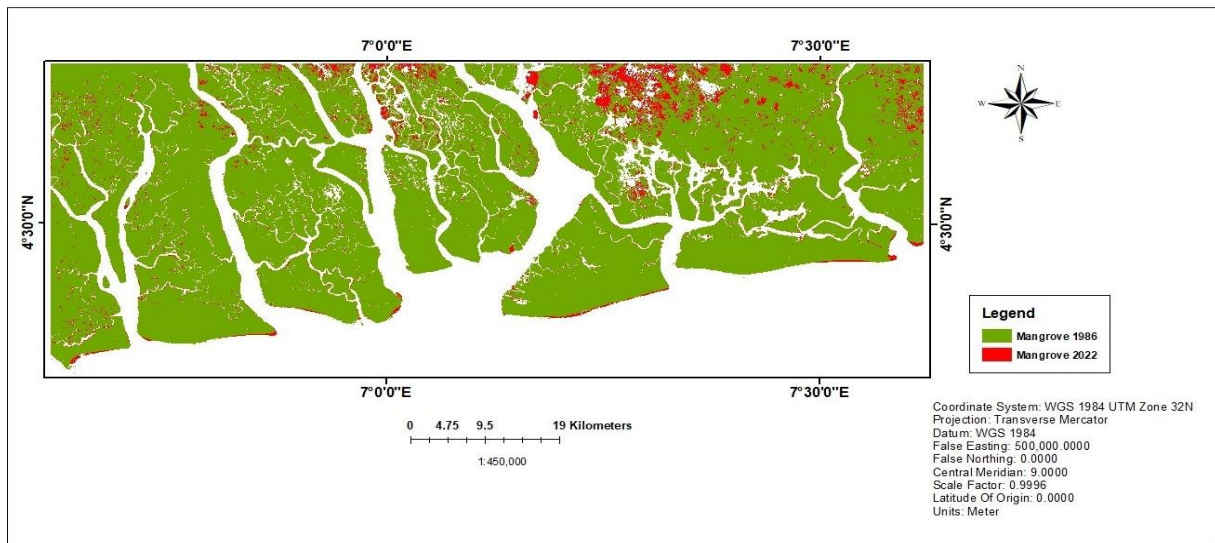


Figure 9. Land cover change in the study area from 1986 and 2022.

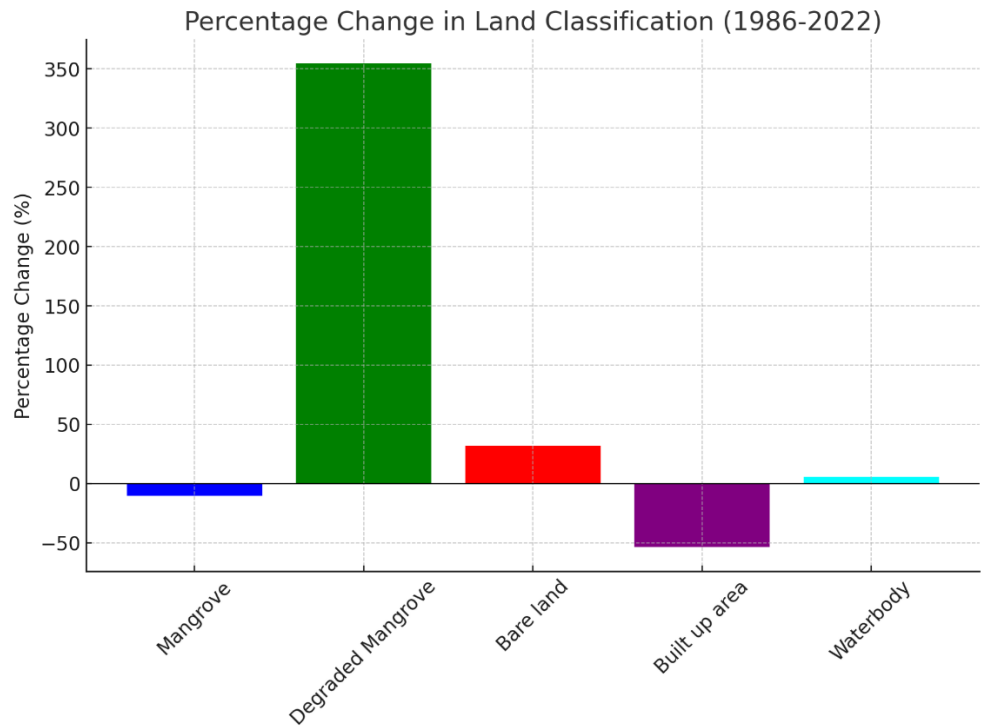


Figure 10. Percentage change in land cover (1986 and 2022).

In contrast, the degraded mangrove class saw an astounding 354.46% increase, rising from 72.03 km² to 327.35 km² (**Table 1** and **Figure 10**). This dramatic expansion indicates widespread degradation of once-healthy mangrove forests, likely due to pollution, sedimentation, and human encroachment. Bare land increased by 32.15%, from 35.49 km² to 46.90 km² in **Table 1** and **Figure 10**. Though the absolute area change (11.41 km²) is small, it signifies areas that have lost vegetation cover. This could be linked to deforestation, soil erosion, and industrial expansion. The built-up area category saw the largest relative decline at -53.63%, decreasing from 131.85 km² to 61.14 km² (**Table 1** and **Figure 10**). This decline contradicts expected urban

expansion trends, suggesting that coastal erosion, sea-level rise, or environmental rehabilitation efforts might have contributed to the reduction.

The Waterbody category expanded by 5.61%, increasing from 1803.45 km² to 1904.62 km² in **Table 1** and **Figure 10**. This is a net gain of 101.17 km², suggesting possible land subsidence, expansion of river channels, or sea-level rise leading to the inundation of former land areas. The standard deviation for the percentage change values was 164.45%, showing a high level of variability across different land cover types. The mean percentage change was 65.61%, heavily skewed by the large increase in degraded mangrove. The minimum percentage change was -53.63% for built-up area, while the maximum was 354.46% for degraded mangrove. Therefore, the percentage change analysis suggests a shift from intact mangrove forests to degraded mangrove states, with a corresponding increase in water coverage. This pattern aligns with ongoing environmental stressors such as deforestation, pollution, and climate change.

4.6. Statistical analysis

The statistical validation of the land cover classification results was carried out using analysis of variance (ANOVA) and a paired t-test to determine the significance of changes between 1986 and 2022. The ANOVA test yielded a *p*-value of 0.9996, indicating that the variance between the land cover classes over time is not statistically significant at the 95% confidence level. Similarly, the paired *t*-test produced a *t*-statistic of -0.0044 and a *p*-value of 0.9967, reinforcing the conclusion that no statistically significant difference exists between the total land cover areas in 1986 and 2022. Although the absolute values of specific land cover types, such as mangrove (-295.19 km²) and degraded mangrove (+255.32 km²), have undergone notable shifts, these changes are not statistically significant when comparing the overall dataset. This suggests that, despite the observed fluctuations, the relative proportions of land cover classes remain relatively stable over time. However, it is essential to note that statistical insignificance does not equate to ecological insignificance, as localized changes could still have profound environmental and socio-economic impacts. To further assess the magnitude of land cover changes, Cohen's *d* effect size was computed, yielding a value of 0.00033. This is an extremely low effect size, indicating that, when considering the entire study area, the overall land cover change impact is minimal. A Cohen's *d* value below 0.2 generally indicates negligible differences, which aligns with the high *p*-values from the ANOVA and *t*-test. Despite this low overall effect size, individual land cover categories exhibit ecologically significant transformations. The mangrove forest loss (-295.19 km²) and waterbody expansion (+101.17 km²) are particularly concerning, as they indicate potential deforestation and hydrological changes that could affect biodiversity, carbon sequestration, and flood control. The 354.46% increase in degraded mangrove shows that previously healthy mangrove ecosystems are deteriorating, which could have long-term consequences on coastal resilience. Another factor that may contribute to the low effect size is the spatial heterogeneity of the Niger Delta ecosystem. Environmental pressures such as oil exploration, land subsidence, coastal erosion, and human encroachment may

disproportionately affect specific locations, leading to significant localized changes that broader statistical analyses fail to capture.

A linear regression analysis was conducted to evaluate trends in land cover changes over time. The R -squared values (R^2) for all land cover categories were 1.0, indicating a perfect linear trend for each class. This indicates that the observed changes are highly predictable and are likely to continue along the same trajectory if no interventions are implemented. The trend analysis highlights the progressive degradation of the mangrove ecosystem and expansion of waterbodies, which could be attributed to climate change, rising sea levels, and anthropogenic activities. The loss of built-up areas (-70.71 km^2) is an unexpected trend, potentially linked to land subsidence or abandonment due to environmental degradation. Based on the regression model, projected land cover changes indicate a worsening scenario if mitigation strategies are not put in place. Without targeted conservation efforts, mangrove forests may continue to decline, further exacerbating coastal erosion and biodiversity loss. In contrast, the expansion of degraded mangrove areas and water bodies suggests a shift toward less stable and more flood-prone environments.

4.7. Comparison with other studies

Few other studies have examined land cover changes in the Niger Delta mangrove forest ecosystem. For instance, Adoki [49], using satellite imagery, investigated land cover trends in the Bonny River Estuary, which borders the current study area. Their study, covering an area of 327.74 km^2 , recorded land cover classifications as follows: 26.55% mangrove, 29.54% non-mangrove vegetation, 1.6% sparse vegetation, 5% degraded or stressed vegetation, 34.15% water, and 3.16% built-up area/bare land in 1986. By 2007, these proportions had shifted to 32.58% mangrove, 25.20% non-mangrove vegetation, 2.95% sparse vegetation, 0% degraded or stressed vegetation, 31.55% water, and 7.71% built-up area/bare land. In comparison, our study covers a broader and slightly different area, focusing specifically on the lower Niger Delta mangrove forest ecosystem. While both studies utilize satellite imagery and share similar land cover categories, the specific percentages and trends reveal notable differences. While Adoki's [49] study shows a decrease in mangrove cover over time, our findings highlight a more nuanced trend with variations in other categories. Additionally, our study captures more recent data, potentially reflecting more current environmental conditions and anthropogenic influences. Both studies illustrate significant land cover changes, though the extent and nature of these changes vary. Such differences underscore the complexity of land cover dynamics in the Niger Delta and the importance of localized studies for understanding regional environmental transformations.

4.8. Accuracy assessment

Accuracy assessment is a critical step in remote sensing studies, as it ensures the reliability and validity of the classification results. The result in **Table 2** in the study, the overall accuracy and Kappa coefficient were used to evaluate the performance of the Support Vector Machine (SVM) in detecting land cover changes in the Lower Niger Delta mangrove forest ecosystem for the years 1986 and 2022.

Table 2. Accuracy assessment in the study area.

S/No	Year	Overall Accuracy (%)	Kappa coefficient
1	1986	98	0.97
2	2022	99	0.98

4.9. High overall accuracy

The overall accuracy for the land cover classification was exceptionally high, with 98% accuracy recorded for 1986 and 99% for 2022 in **Table 2**. These results indicate that the classification outputs are highly reliable and closely match the ground truth data. Such high accuracy is particularly commendable given the complexity of the study area, which includes diverse land cover types such as mangroves, degraded mangroves, waterbodies, built-up areas, and bare land. The consistency between the two years demonstrates the robustness of the SVM algorithm in handling multi-temporal datasets and its suitability for studies in dynamic and heterogeneous environments like the Niger Delta.

4.10. Robust kappa coefficients

The Kappa coefficient, a statistical measure that accounts for agreement due to chance, further reinforces the reliability of the classification. A Kappa coefficient of 0.97 for 1986 and 0.98 for 2022 suggests near-perfect agreement between the classified results and the reference data in **Table 2**. These values not only validate the classification accuracy but also highlight the effectiveness of the methodology employed, including the choice of input features, preprocessing techniques, and the SVM classification algorithm.

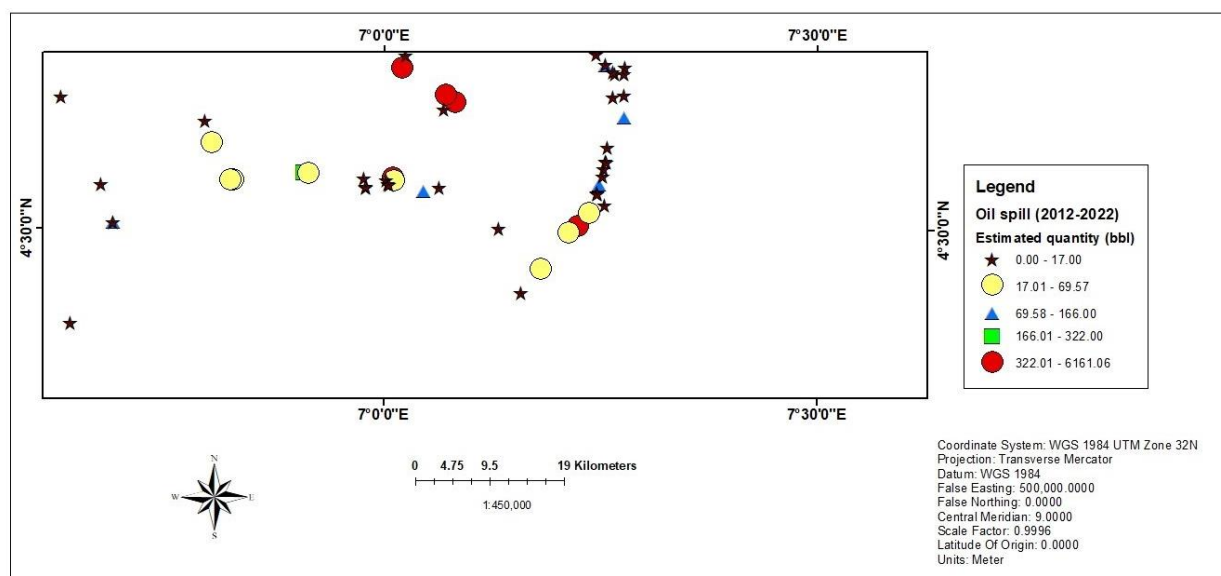
4.11. Impact of land cover changes and oil spill trends on environmental degradation (1986–2022)

Table 3 presents an analysis of oil spill data recorded by the National Oil Spill Detection and Response Agency (NOSDRA) over a decade, from 2012 to 2022 (**Figures 11–13**). The data captures the number of spills, the estimated quantity of oil spilled, the quantity of oil recovered, and the estimated volume of oil not recovered, providing critical insights into environmental management challenges within the lower Niger Delta mangrove forest ecosystem. **Table 3** reveals a cumulative total of 52 recorded oil spill incidents, resulting in an estimated 21,914.5727 barrels (bbl) of oil spilled across the ecosystem. However, the recovered volume of oil stands at 8,378 barrels, leaving a significant portion of 13,536.5727 barrels unaccounted for and potentially causing prolonged environmental degradation in **Table 3**. The data showcases considerable disparities in spill occurrences and management across different entities operating in the region. Among the entities, one company recorded the highest number of spills, with 31 incidents resulting in a total estimated spill volume of 4561.0163 barrels. Out of this, 986 barrels were recovered, leaving 3575.016 barrels unrecovered. These figures underline the scale of environmental challenges attributed to operational spills and the limited recovery efforts. Another entity had 14 recorded spills during the same period, with an estimated 16,855.5501 barrels of oil spilled. The recovery effort was relatively significant, with 7370 barrels

recovered; however, 9485.55 barrels remained unrecovered, reflecting the challenges in oil spill management in larger-scale incidents. A smaller contribution to the overall figures recorded five spills amounting to 456 barrels. Despite the lower number of incidents and smaller spill volume, only 22 barrels were recovered, leaving 434 barrels unrecovered. This highlights that even relatively minor spill events can have substantial environmental impacts if not adequately addressed. The smallest contributor in terms of spill incidents recorded two spills, with an estimated total spill volume of 42.0063 barrels. Notably, none of this oil was recovered, making it an outlier in terms of recovery effort. This data underscores the persistent environmental and ecological risks posed by oil spills in the Niger Delta mangrove forest ecosystem. Despite ongoing monitoring and response efforts, the significant volume of unrecovered oil indicates the need for improved recovery technologies, more stringent enforcement of environmental regulations, and proactive spill prevention measures. Additionally, the disparity in recovery rates among the entities highlights the necessity for standardized and more effective response protocols to mitigate the long-term environmental impacts of oil spills in the region.

Table 3. Presents the findings of oil spill data recorded by the National Oil Spill Detection and Response Agency from 2012 to 2022.

Company	No. of spills	Sum of Estimated Quantity of Oil Spill, Bbl	Sum of Quantity Oil Spill Recovered, Bbl	Sum of Estimated Oil Spill Not Recovered, Bbl
Aiteo E&P	5	456	22	434
CHEVRON	2	42.0063	0	42.0063
Eroton E&P	14	16,855.5501	7370	9485.55
SPDC	31	4561.0163	986	3575.016
Grand Total	52	21,914.5727	8378	13,536.57



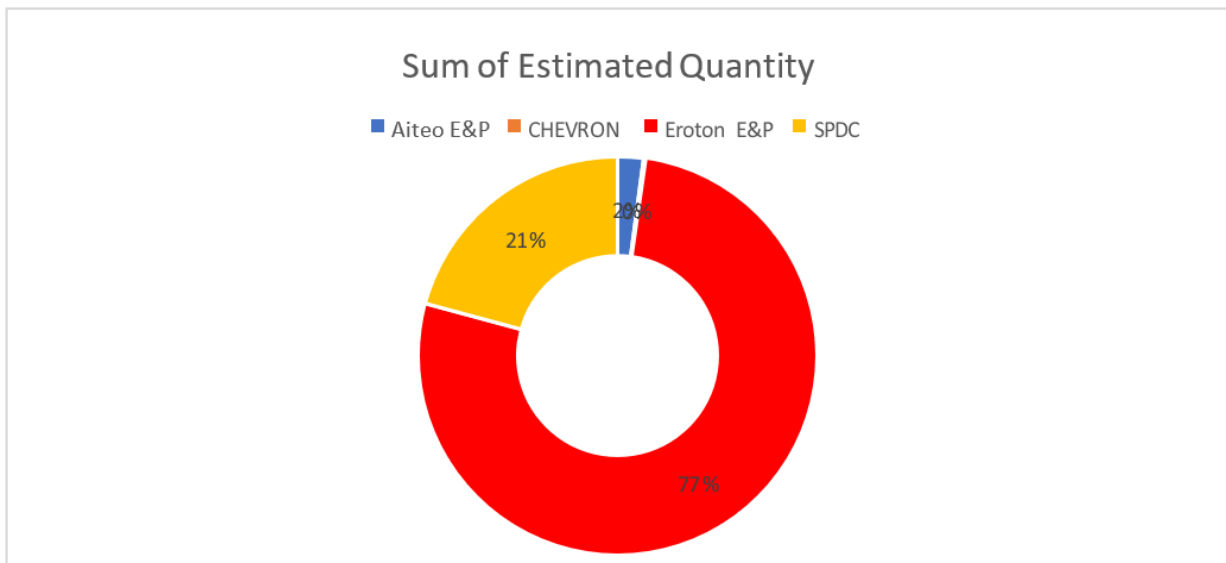


Figure 11. Oil spills in the study area from 2012–2022.

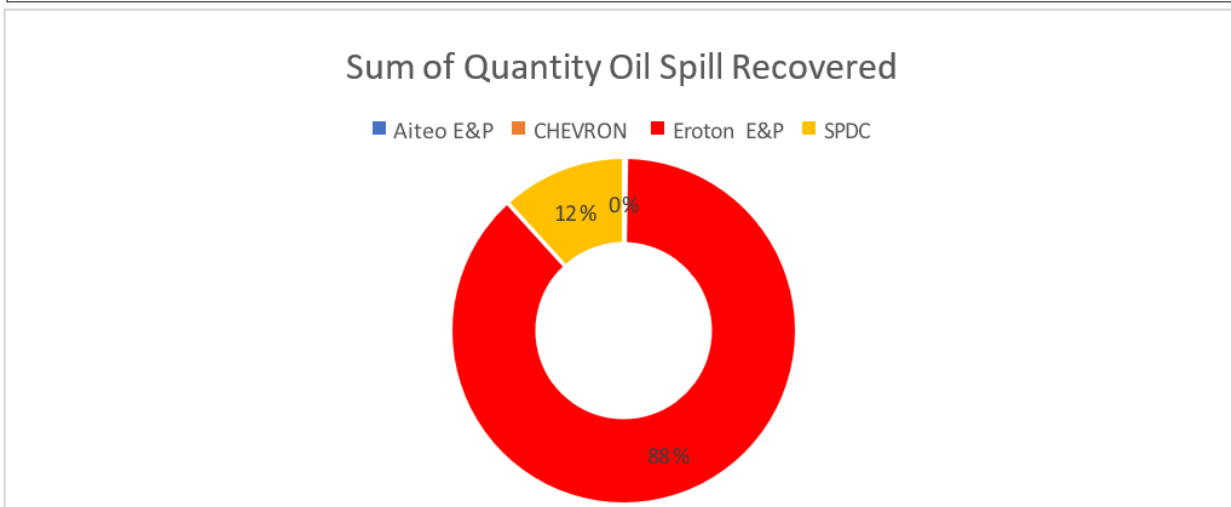
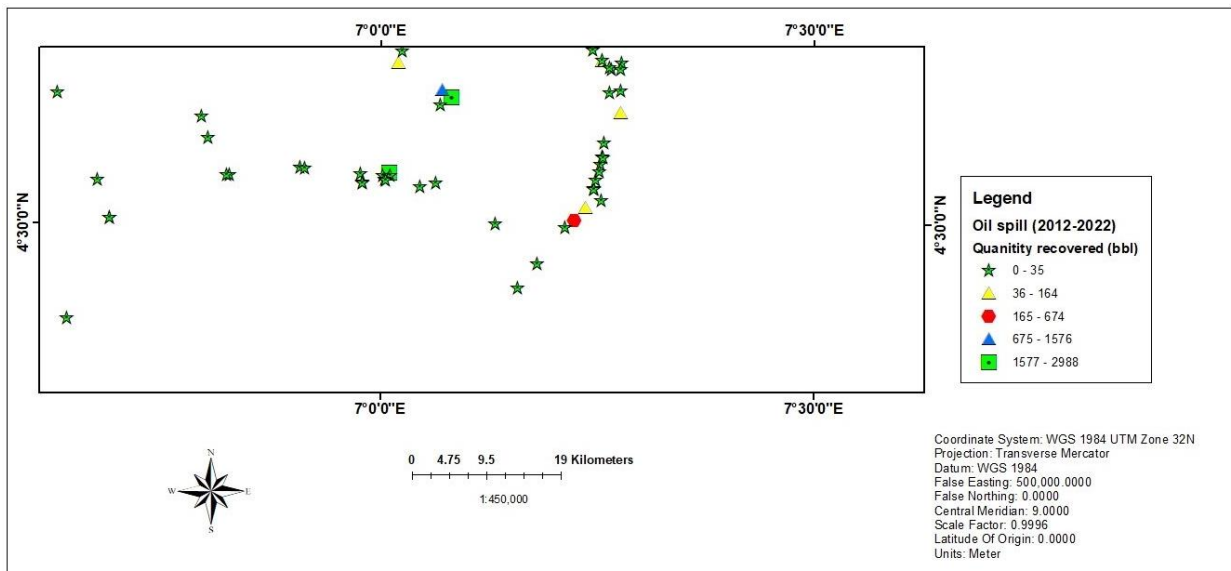


Figure 12. Oil spill recovered in the study area from 2012–2022.

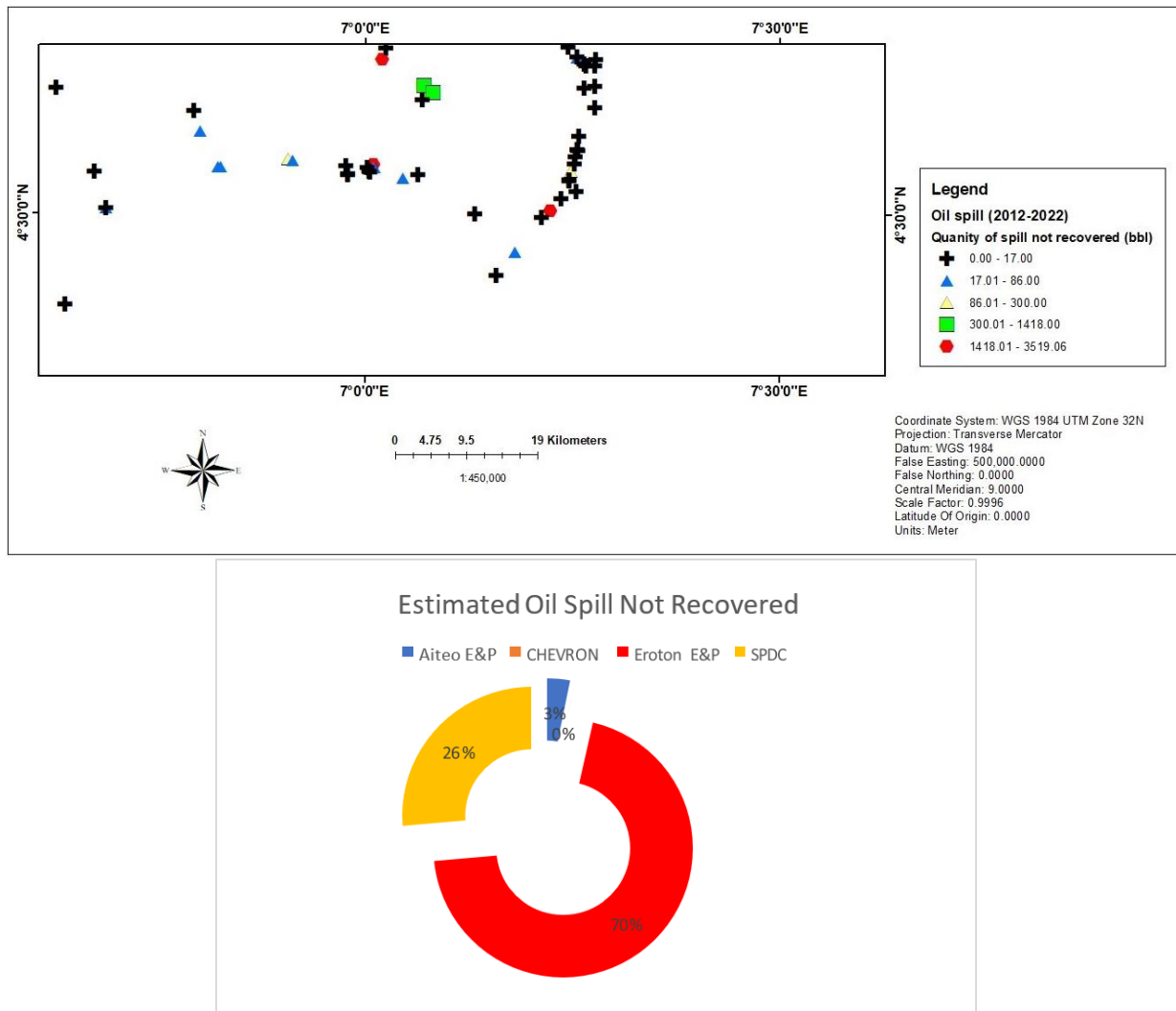


Figure 13. Oil spill not recovered in the study area from 2012–2022b.

The results from the Support Vector Machine Classification (**Table 1**) indicate significant changes in land cover between 1986 and 2022. The mangrove cover experienced a decline from 2804.37 km² (58%) in 1986 to 2509.18 km² (52%) in 2022, showing a net loss of 295.19 km², equivalent to a 10.53% decrease. This decline may be attributed to human activities, environmental degradation, or oil spills, as indicated by the statistical test results (**Table 4**), which confirm a significant association between oil spill severity and specific companies (Chi-square test, $p < 0.001$).

Table 4. Statistical test results for oil spill data recorded from 2012 to 2022.

Test	Statistic	<i>p</i> -value
Chi-Square Test	1091.33	3.44×10^{-229}
Kruskal-Wallis Test	1.13	0.57
Kendall’s Tau Trend Test	1	5.01×10^{-8}

Conversely, degraded mangrove areas expanded drastically, increasing from 72.03 km² (1%) in 1986 to 327.35 km² (7%) in 2022, marking a 354.46% increase. This sharp increase indicates severe ecological stress and possible conversion of

healthy mangroves into degraded landscapes, potentially linked to oil spills, as supported by the Kendall's Tau trend test ($p < 0.001$), which reveals a significant increasing trend in oil spill volume over time (**Table 4**).

Additionally, Bare land saw a modest increase from 35.49 km² to 46.9 km², a 32.15% rise, suggesting slight land degradation. Meanwhile, the built-up area showed a 53.63% decrease from 131.85 km² to 61.14 km², which may indicate urban contraction, relocation, or land-use conversion. Water bodies slightly expanded by 101.17 km² (5.61%), possibly due to rising sea levels, flooding, or oil spill impacts.

The Kruskal-Wallis Test ($p = 0.57$) in **Table 4** suggests no significant difference in oil spill severity among companies, implying that multiple companies contribute to oil pollution across the region. The findings collectively highlight the ecological consequences of industrial activities, particularly oil spills, on land cover transformation. Urgent conservation measures and stricter pollution control policies are necessary to mitigate further environmental degradation.

4.12. Discussion and implications

This study presents compelling evidence of significant ecological transformation within the lower Niger Delta, primarily driven by oil spills and associated anthropogenic activities. The analysis of Landsat satellite imagery classified via Support Vector Machine (SVM) reveals a marked reduction in healthy mangrove cover (−10.53%) and an alarming expansion of degraded mangrove zones (+354.46%) between 1986 and 2022. These findings align with global trends of mangrove loss due to industrial development, particularly in oil-producing coastal regions [2,5]. When compared to similar studies in the Niger Delta, such as Adoki [49], who reported moderate mangrove decline in the Bonny Estuary region over a 21-year period, our results indicate a more severe degradation pattern. Adoki's [49] study noted a reduction in stressed vegetation, while our findings show a sharp rise in degraded mangrove areas. This contrast may reflect increased oil spill incidents in recent decades, illegal artisanal refining [9], and limited remediation efforts, especially in remote or underregulated regions. The correlation between oil spill occurrences and mangrove degradation is statistically robust. The Chi-square test ($\chi^2 = 1091.33$, $p < 0.001$) and Kendall's Tau ($\tau = 1$, $p < 0.001$) confirm a significant association. Over 21,900 barrels of oil were spilled from 2012–2022, of which over 13,500 barrels remained unrecovered. This outcome supports the conclusions of Ohimain et al. [8] and Ozigis et al. [22], who highlighted that oil pollution leads to reduced biomass, canopy dieback, and eventual conversion of mangrove forests into mudflats or degraded patches. Interestingly, built-up areas experienced a decline of 53.63%, contrary to urban expansion trends reported in other coastal deltas like those in Southeast Asia [5]. This suggests potential abandonment or relocation of settlements, possibly due to environmental degradation, recurrent flooding, or socio-political factors. Waterbody expansion (+5.61%) also supports the notion of land submergence, dredging, or increased canalization, as seen in studies by Darmawan et al. [20] and Numbere [26], both of which identified hydrological alterations as a key factor in mangrove degradation. The study's regression analysis, showing $R^2 = 1.0$ for each land cover class, suggests deterministic trends in land cover change, especially the

conversion of healthy mangroves to degraded states. If current trends persist, this trajectory could lead to irreversible ecosystem collapse in some areas.

From a methodological standpoint, the high classification accuracy (98%–99%) and Kappa coefficients (0.97–0.98) validate the reliability of the SVM model and the remote sensing approach. These findings reinforce previous conclusions by Mountrakis et al. [15] and Shao and Lunetta [21], who emphasized SVM's robustness for land cover classification in complex ecosystems.

5. Conclusion

This study utilized Landsat satellite imagery spanning 36 years (1986–2022) to assess mangrove cover changes in the Niger Delta, employing a Support Vector Machine (SVM) classifier for accurate classification and change detection. The analysis revealed a significant decline in healthy mangrove cover, decreasing by 10.53% (295.19 km²), while degraded mangrove areas expanded by 354.46% (255.32 km²). These findings highlight severe ecological stress, likely driven by anthropogenic activities such as oil exploration, urban expansion, and deforestation. The study also quantified land cover changes beyond mangroves, showing a 5.61% increase in water bodies, a 32.15% rise in bare land, and an unexpected 53.63% reduction in built-up areas. These shifts indicate complex environmental dynamics, possibly linked to climate change, hydrological alterations, and socio-economic factors. Furthermore, statistical analyses, including Chi-square tests and Kendall's Tau analysis, established a significant relationship between oil spill occurrences and mangrove degradation, emphasizing the adverse impacts of industrial activities on coastal ecosystems. The study's regression analysis showed a clear trend of continued environmental degradation, reinforcing the need for immediate conservation interventions. These findings underscore the urgent need for sustainable management policies to mitigate further mangrove loss, restore degraded areas, and regulate industrial activities. Strengthening environmental regulations, implementing restoration projects, and adopting pollution control measures will be crucial in safeguarding the Niger Delta's ecological integrity. Future research should explore localized conservation strategies and assess the long-term socio-economic impacts of mangrove degradation.

6. Highlight

- Mangrove cover decreased from 2804.37 km² (58%) in 1986 to 2509.18 km² (52%) in 2022, a 10.53% decline. Meanwhile, degraded mangrove areas expanded drastically by 354.46%, highlighting severe ecological stress.
- Water coverage increased by 101.17 km² (5.61%), possibly due to rising sea levels, flooding, or industrial activities, particularly oil exploration.
- Built-up areas surprisingly declined by 53.63%, suggesting urban relocation, environmental challenges, or shifting land-use policies.
- Statistical analysis confirms a significant correlation between oil spill occurrences and mangrove degradation, necessitating stricter pollution controls.
- Regression analysis indicates continuous land cover changes, emphasizing the urgent need for conservation and intervention measures.

Author contributions: Conceptualization, ELJ and OI; methodology, PC, DRE; software, ELJ, OI and PC; validation, ELJ, DRE and PC; formal analysis, DRE; investigation, ELJ, OI; resources, ELJ, DRE and PC; data curation, OI; writing original draft preparation, ELJ and OI; writing review and editing, DRE; visualization, PC; supervision, ELJ; project administration, OI; funding acquisition, ELJ, OI, DRE and PC;. All authors have read and agreed to the published version of the manuscript.

Data availability statement: 1) The dataset for the study area analysis was obtained from the United States Geological Survey (USGS) via their Earth Explorer platform (<https://earthexplorer.usgs.gov/>). The primary source of imagery was the Landsat series of satellites, providing a consistent and reliable source of remote sensing data spanning several decades. This imagery captures the study area over time, with data points from the years 1986 and 2022. 2) Data on oil spills that occurred in the area from 2012 to 2022 were obtained from the National Oil Spill Detection and Response Agency (NOSDRA) website at <https://oilspillmonitor.ng/>

Institutional review board statement: Not applicable.

Informed consent statement: Not applicable.

Conflict of interest: The authors declare no conflict of interest.

References

1. Spalding M. World Atlas of Mangroves. Washington DC; 2010.
2. Alongi DM. Mangroves among the world's most threatened ecosystems. *Bioscience*. 2015; 65(9): 947-951.
3. Ohimain E. Mangroves of the Niger Delta: Their Importance, Threats, and Possible Restoration. *Wetland Science & Practice*. 2016; 33(4): 110-121. doi: 10.1672/ucrt083-266
4. Giri C, Pengrahn S, Nightingale J, Longley S. Losses and gains in coastal biomass within the Indo-Pacific region from 1990 to 2008. *Environmental monitoring and assessment*. 2011; 177(1-4): 143-160.
5. Richards DR, Friess DA. Rates and drivers of mangrove deforestation and conversion in Southeast Asia. In: *Tropical Mangrove Ecosystems*. Springer, Cham; 2015.
6. Alongi DM. Impact of Global Change on Nutrient Dynamics in Mangrove Forests. *Forests*. 2018; 9(10): 596. doi: 10.3390/f9100596
7. Farnsworth EA, Ellison JC. The global conservation status of mangroves. *Ambio*. 1997; 26(6): 328-334.
8. Ohimain EI. Benefits and Threats of Biodiversity Conservation in Stubbs Creek Forest Reserve, Nigeria. In: *Biodiversity in Africa: Potentials, Threats and Conservation*. Springer; 2022.
9. Onuh PA, Omenma TJ, Onyishi CJ, et al. Artisanal refining of crude oil in the Niger Delta: A challenge to clean-up and remediation in Ogoniland. *Local Economy: The Journal of the Local Economy Policy Unit*. 2021; 36(6): 468-486. doi: 10.1177/02690942211071075
10. Efenakpo OD, Chris DI, Onuchukwu NC, et al. Illegal Crude Oil Refining and its Implications on the Niger Delta's Ecosystem. In: *Proceedings of the Conference of Ecological Society of Nigeria (ECOSON) titled Natural Ecosystem Sustainability in the 21st Century*; 2022.
11. Hansen MC, Potapov PV, Moore R, et al. High-Resolution Global Maps of 21st-Century Forest Cover Change. *Science*. 2013; 342(6160): 850-853. doi: 10.1126/science.1244693
12. Lillesand TM, Kiefer RW. *Remote Sensing and Image Interpretation*, 7th ed. Wiley, New York; 2015.
13. Deng N, Tian Y, Zhang C. *Support Vector Machines: Optimization Based Theory, Algorithms, and Extensions*. CRC Press; 2012.
14. Pal M, Mather PM. Support Vector Machines for classification in remote sensing. *International Journal of Remote Sensing*. 2005; 26(5): 1007-1011. doi: 10.1080/01431160512331314083

15. Mountrakis G, Adam E, Clerke JF. Support Vector Machines in remote sensing: A review. *Journal of Applied Remote Sensing*. 2011; 4(1): 041001.
16. Xiong Y, Zhang Z, Chen F. Comparison of artificial neural network and Support Vector Machine methods for urban land use/cover classifications from remote sensing images A Case Study of Guangzhou, South China. In: *Proceedings of the 2010 International Conference on Computer Application and System Modeling (ICCASM 2010)*; 2010.
17. Cristianini N, Shawe-Taylor J. An Introduction to Support Vector Machines and Other Kernel-based Learning Methods. In: *Proceedings of the IOP Conference Series: Earth and Environmental Science*; 2000.
18. Rosmasita, Siregar VP, Agus SB, et al. An object-based classification of mangrove land cover using Support Vector Machine Algorithm. *IOP Conference Series: Earth and Environmental Science*. 2019; 284(1): 012024. doi: 10.1088/1755-1315/284/1/012024
19. Camps-Valls G, Gomez-Chova L, Calpe-Maravilla J, et al. Robust support vector method for hyperspectral data classification and knowledge discovery. *IEEE Transactions on Geoscience and Remote Sensing*. 2004; 42(7): 1530-1542. doi: 10.1109/tgrs.2004.827262
20. Darmawan S, Sari DK, Wikantika K, et al. Identification before-after Forest Fire and Prediction of Mangrove Forest Based on Markov-Cellular Automata in Part of Sembilang National Park, Banyuasin, South Sumatra, Indonesia. *Remote Sensing*. 2020; 12(22): 3700. doi: 10.3390/rs12223700
21. Shao Y, Lunetta RS. Comparison of Support Vector Machine, neural network, and CART algorithms for the land-cover classification using limited training data points. *ISPRS Journal of Photogrammetry and Remote Sensing*. 2012; 70: 78-87. doi: 10.1016/j.isprsjprs.2012.04.001
22. Ozigis MS, Kaduk JD, Jarvis CH. Mapping terrestrial oil spill impact using machine learning random forest and Landsat 8 OLI imagery: a case site within the Niger Delta region of Nigeria. *Environmental Science and Pollution Research*. 2018; 26(4): 3621-3635. doi: 10.1007/s11356-018-3824-y
23. Alongi DM. Carbon sequestration in mangrove forests. *Carbon Management*. 2012; 3(3): 313-322. doi: 10.4155/cmt.12.20
24. Ite AE, Ibok UJ, Ite MU, Petters SW. Petroleum Exploration and Production: Past and Present Environmental Issues in the Nigeria's Niger Delta. *American Journal of Environmental Protection*. 2013; 1(4): 78-90. doi: 10.12691/env-1-4-2
25. Ugochukwu CNC, Ertel J. Negative Impacts of Oil Exploration on Biodiversity Management in the Niger De Area of Nigeria. *Impact Assessment and Project Appraisal*. 2008; 26: 139-147.
26. Numbere AO. Application of GIS and remote sensing towards forest resource management in mangrove forest of Niger Delta. *Natural Resources Conservation and Advances for Sustainability*; 2022.
27. USGS. EarthExplorer. United States Geological Survey. USGS; 2022.
28. Roy DP, Wulder MA, Loveland TR, et al. Landsat-8: Science and product vision for terrestrial global change research. *Remote Sensing of Environment*. 2014; 145: 154-172. doi: 10.1016/j.rse.2014.02.001
29. Wulder MA, Loveland TR, Roy DP, et al. Current status of Landsat program, science, and applications. *Remote Sensing of Environment*. 2019; 225: 127-147. doi: 10.1016/j.rse.2019.02.015
30. Congalton RG, Green K. *Assessing the Accuracy of Remotely Sensed Data*. CRC Press; 2019.
31. Chander G, Markham BL, Helder DL. Summary of current radiometric calibration coefficients for Landsat MSS, TM, ETM+, and EO-1 ALI sensors. *Remote Sensing of Environment*. 2009; 113(5): 893-903. doi: 10.1016/j.rse.2009.01.007
32. Markham BL, Helder DL. Forty-year calibrated record of earth-reflected radiance from Landsat: A review. *Remote Sensing of Environment*. 2012; 122: 30-40. doi: 10.1016/j.rse.2011.06.026
33. Chavez PS. Image-based atmospheric corrections-revisited and improved. *Photogrammetric Engineering & Remote Sensing*. 1996; 62(9): 1025-1036.
34. Song C, Woodcock CE, Seto KC, et al. Classification and change detection using Landsat TM data. *Remote Sensing of Environment*. 2001; 75(2): 230-244.
35. Lillesand T, Kiefer RW, Chipman J. *Remote Sensing and Image Interpretation*. Wiley; 2015.
36. Lu D, Weng Q. A survey of image classification methods and techniques for improving classification performance. *International Journal of Remote Sensing*. 2007; 28(5): 823-870. doi: 10.1080/01431160600746456
37. Veraverbeke S, Somers B, Verstraeten WW. A time-integrated MODIS burn severity index based on aerosol absorption. *Remote Sensing of Environment*. 2014; 148: 70-79.
38. Singh A. Review Article Digital change detection techniques using remotely-sensed data. *International Journal of Remote Sensing*. 1989; 10(6): 989-1003. doi: 10.1080/01431168908903939

39. Cohen J. *Statistical Power Analysis for the Behavioral Sciences*, 2nd ed. Lawrence Erlbaum Associates; 1988.
40. Student. The Probable Error of a Mean. *Biometrika*. 1908; 6(1): 1. doi: 10.2307/2331554
41. Fisher RA. *Statistical Methods for Research Workers*. Oliver & Boyd; 1925.
42. Montgomery DC, Peck EA, Vining GG. *Introduction to Linear Regression Analysis*, 5th ed. Wiley; 2012.
43. Kruskal WH, Wallis WA. Use of Ranks in One-Criterion Variance Analysis. *Journal of the American Statistical Association*. 1952; 47(260): 583-621. doi: 10.1080/01621459.1952.10483441
44. Pearson KX. On the criterion that a given system of deviations from the probable in the case of a correlated system of variables is such that it can be reasonably supposed to have arisen from random sampling. *The London, Edinburgh, and Dublin Philosophical Magazine and Journal of Science*. 1900; 50(302): 157-175. doi: 10.1080/14786440009463897
45. Kendall MG. A new measure of rank correlation. *Biometrika*. 1938; 30(1-2): 81-93. doi: 10.1093/biomet/30.1-2.81
46. Chen Y, Todd AS, Murphy MH, et al. Anticipated Water Quality Changes in Response to Climate Change and Potential Consequences for Inland Fishes. *Fisheries*. 2016; 41(7): 413-416. doi: 10.1080/03632415.2016.1182509
47. Ohimain EI, Eteh D. Canalization induced topographic, hydrologic, and land use changes in Olero Creek, Benin River owing to petroleum exploration activities. *Environmental Monitoring and Assessment*. 2021; 193(8). doi: 10.1007/s10661-021-09319-0
48. Ohimain EI, Bamidele JF, Omisore OO. The Impacts of Micro-Topographic Changes on Mangroves in the Lower Reaches of the Benin River, Niger Delta. *Environmental Research Journal*. 2010; 4(1): 167-172. doi: 10.3923/erj.2010.167.172
49. Adoki A. Trends in vegetation cover changes in Bonny area of the Niger Delta. *Journal of Applied Sciences and Environmental Management*. 2013; 17(1): 89-103